August 5, 2011

Discrete breathers in a nonlinear electric line: Modeling, computation, and experiment

F. Palmero
L. Q. English
J. Cuevas
R. Carretero-Gonz´alez
Panos Kevrekidis

Discrete breathers in a nonlinear electric line: Modeling, computation, and experiment

F. Palmero,[1,*] L. Q. English,[2] J. Cuevas,[3] R. Carretero-González,[4,†] and P. G. Kevrekidis[5]

[1]*Nonlinear Physics Group, Escuela Técnica Superior de Ingeniería Informática, Departamento de Física Aplicada I, Universidad de Sevilla, Avda. Reina Mercedes, s/n, E-41012 Sevilla, Spain*

[2]*Department of Physics and Astronomy, Dickinson College, Carlisle, Pennsylvania 17013, USA*

[3]*Grupo de Física No Lineal, Departamento de Física Aplicada I, Escuela Politécnica Superior, Universidad de Sevilla, C/ Virgen de África, 7, E-41011 Sevilla, Spain*

[4]*Nonlinear Dynamical Systems Group, Department of Mathematics and Statistics and Computational Science Research Center, San Diego State University, San Diego, California 92182-7720, USA*

[5]*Department of Mathematics and Statistics, University of Massachusetts, Amherst, Massachusetts 01003-4515, USA*

(Received 15 April 2011; published 5 August 2011)

We study experimentally and numerically the existence and stability properties of discrete breathers in a periodic nonlinear electric line. The electric line is composed of single cell nodes, containing a varactor diode and an inductor, coupled together in a periodic ring configuration through inductors and driven uniformly by a harmonic external voltage source. A simple model for each cell is proposed by using a nonlinear form for the varactor characteristics through the current and capacitance dependence on the voltage. For an electrical line composed of 32 elements, we find the regions, in driver voltage and frequency, where n-peaked breather solutions exist and characterize their stability. The results are compared to experimental measurements with good quantitative agreement. We also examine the spontaneous formation of n-peaked breathers through modulational instability of the homogeneous steady state. The competition between different discrete breathers seeded by the modulational instability eventually leads to stationary n-peaked solutions whose precise locations is seen to sensitively depend on the initial conditions.

DOI: 10.1103/PhysRevE.84.026605 PACS number(s): 05.45.Yv, 63.20.Pw, 63.20.Ry

I. INTRODUCTION

Nonlinear physics of discrete systems has witnessed enormous development in the past years. In particular, a great deal of attention has been paid to the existence and properties of intrinsic localized modes (ILMs), or discrete breathers, which result from the combination of nonlinearity and spatial discreteness. These spatially localized states have been observed in a wide variety of different systems [1,2]. They were originally suggested as excitations of anharmonic nonlinear lattices [3], but the rigorous proof of their persistence under general conditions [4] led to their investigation in a diverse host of applications. These include, among others, antiferromagnets [5], charge-transfer solids [6], photonic crystals [7], superconducting Josephson junctions [8], micromechanical cantilever arrays [9], granular crystals [10], and biopolymers [11]. More recently, the direct manipulation and control of such states has been enabled through suitable experimental techniques [12].

Despite the tremendous strides made in this field, the relevant literature, nevertheless, often appears to be quite sharply divided between theory and experiment. Frequently experimental studies do not capture the dynamics in enough detail to facilitate an exact comparison with theoretical studies. At other times, the theoretical models are not refined enough (or lack the inclusion of nontrivial experimental factors some of which may be difficult to quantify precisely) to make quantitative contact with the experimental results. Our system—a macroscopic electrical lattice in which solitons have a time-honored history [13,14]—is, arguably, ideally suited for this kind of cross comparison: the lattice dynamics can be measured fully in space and time, and the physical properties of individual unit cells of the lattice can be characterized in enough detail to allow for the construction of effective models.

In this paper we present a detailed study of discrete breathers in an electric lattice in which ILMs have been experimentally observed [15–17]. We propose a theoretical model which allows us to systematically study their existence, stability and properties, and to compare our numerical findings with experimental results. We demonstrate good agreement not only at a qualitative but also at a quantitative level between theory and experiment. The presentation of our results is organized as follows. In the next section we study the characteristics (intensity and capacitance curves versus voltage) of the varactor, the nonlinear circuit element, in order to develop the relevant model for the electrical unit cell. The results for the single cell are validated through the comparison of its resonance curves for different driving strengths. We also derive the equations describing the entire electrical line. In Sec. III we study the existence and stability properties of n-peaked breathers for $n = 1, 2, 3$ in the driving frequency and voltage parameter space. The numerical results are compared to the experimental data with good quantitative agreement. We also briefly study the spontaneous formation of n-peaked breathers from the modulational instability of the homogeneous steady state. We observe that the location and number of the final peaks depends sensitively on the initial conditions. Finally, in Sec. IV, we conclude our manuscript and offer some suggestions for possible avenues of further research.

II. THEORETICAL SETUP

Our system consists on an electric line as represented in Fig. 1. This line can be considered as a set of single cells, each

*palmero@us.es

†[http://nlds.sdsu.edu]

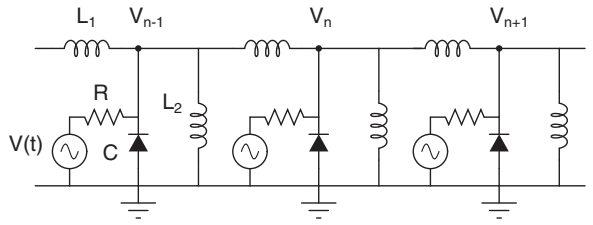

FIG. 1. Schematic circuit diagram of the electrical transmission line.

one composed of a varactor diode (NTE 618) and an inductor $L_2 = 330\ \mu$H, coupled through inductors $L_1 = 680\ \mu$H. Each unit cell or node is driven via a resistor, $R = 10$ kΩ, by a sinusoidal voltage source $V(t)$ with amplitude V_d and frequency f. In experiments a set of 32 elements has been used, with a periodic ring structure (the last element is connected to the first one), and measurements of voltages V_n have been recorded. Related to the voltage source, we have considered amplitudes from $V_d = 1$ V to $V_d = 5$ V and frequencies from $f = 200$ kHz to $f = 600$ kHz.

In order to propose a set of equations to characterize the electrical line, we have used circuit theory and Kirchhoff's rules; the main challenge has been to describe appropriately each element. In general, resistance and inductors are inherently imperfect impedance components, that is, they have series and parallel, reactive, capacitive, and resistive elements. Moreover, due to the commercial nature of the elements, manufactured components are subject to tolerance intervals, and the resultant small spatial inhomogeneity introduces some additional uncertainty. We have quantified the spatial inhomogeneity by separately measuring all lattice components. The diode capacitance was found to vary by 0.3% (standard deviation), whereas the inductors both exhibited a 0.5% variation. Additional factors that may contribute slightly to inhomogeneities are wire inductances as well as load and contact resistances. The varactors (diodes) we use are typically intended for AM receiver electronics and tuning applications. As described later, we characterize this lattice element in more detail, since it is the source of the nonlinearity in the lattice. For such small spreads we consider the lattice sufficiently homogeneous, so that the localization is controlled by the nonlinearity and not by disorder. This assumption is validated by the fact that we do not see localization in the linear regime (for low driver amplitudes). It is also corroborated *a posteriori* below by the direct comparison of our numerical results in a homogeneous lattice with the experimental observations in the very weakly heterogeneous circuit.

As a guiding principle we are aiming to construct a model which is as simple as possible, with a limited number of parameters whose values are experimentally supported, but one which is still able to reproduce the main phenomenon, namely nonlinear localization and the formation of discrete breathers. With this balance in mind, we proceed as follows.

In the range of frequencies studied it is a good approximation to describe the load resistance as a simple resistor, neglecting any capacitive or inductive contribution. Also,

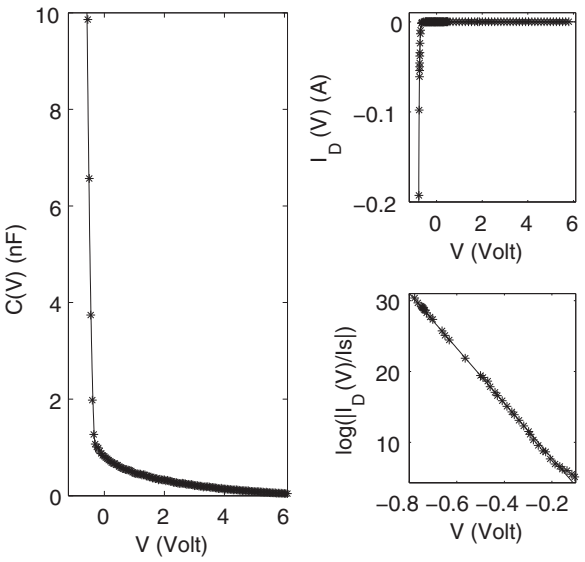

FIG. 2. Experimental data (∗) and numerical approximation thereof (continuous line) corresponding to $C(V)$ and $I_D(V)$ (linear and semilog plots) for the nonlinear varactor.

we have performed experimental measures of the varactor characteristics. This experimental data shows that it can be modeled as a nonlinear resistance in parallel with a nonlinear capacitance, where the nonlinear current $I_D(V)$ is given by

$$I_D(V) = -I_s \exp(-\beta V), \tag{1}$$

where $\beta = 38.8\ \text{V}^{-1}$ and $I_s = 1.25 \times 10^{-14}$ A (we consider negative voltage when the varactor is in direct polarization), and its capacitance as

$$C(V) = \begin{cases} C_v + C_w(V') + C(V')^2 & \text{if} \quad V \leqslant V_c, \\ C_0 e^{-\alpha V} & \text{if} \quad V > V_c, \end{cases} \tag{2}$$

where $V' = (V - V_c)$, $C_0 = 788$ pF, $\alpha = 0.456\ \text{V}^{-1}$, $C_v = C_0 \exp(-\alpha V_c)$, $C_w = -\alpha C_v$ (the capacitance and its first derivative are continuous in $V = V_c$), $C = 100$ nF and $V_c = -0.28$ V. In Fig. 2 we present the experimental data and their corresponding numerical approximations for $I_D(V)$ and $C(V)$, where a good agreement between the two can be observed.

With respect to the inductors, in the range of frequencies considered, capacitive effects are negligible, but they possess a small dc ohmic resistance which is around 2 Ω. The inductors and the varactor are a source of damping in the ac regime, and these contributions must be taken into account. However, we have no manufacturer data related to dissipation parameters, and it is difficult to measure them experimentally. In order to introduce these effects, we will model dissipation phenomenologically by means of a global term given by a resistance R_l, which appears in each unit cell in parallel with L_2; to determine its value, we have studied experimentally a single element as shown in Fig. 3. In this way we will consider the inductors themselves as ideal elements.

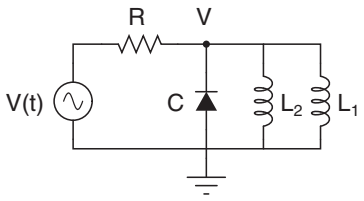

FIG. 3. Single cell element model.

Using basic circuit theory, the single element is described by the equations

$$\frac{dv}{d\tau} = \frac{1}{c(v)}\left[\frac{\cos(\Omega\tau)}{RC_0\omega_0} - \frac{1}{\omega_0 C_0}\left(\frac{1}{R_l}+\frac{1}{R}\right)v + (y - i_D)\right], \tag{3}$$

$$\frac{dy}{d\tau} = -\left(1+\frac{L_2}{L_1}\right)v, \tag{4}$$

where dimensionless variables have been used: $\tau = \omega_0 t$, $i_D = I_D/(\omega_0 C_0 V_d)$, $v = V/V_d$, the dimensionless voltage at point A, $c(v) = C(V)/C_0$, $\Omega = \omega/\omega_0$, and $\omega_0 = 1/\sqrt{L_2 C_0}$; y represents the normalized current through the inductors.

We can generate theoretical nonlinear resonance curves and, comparing with experimental data, select the optimal dissipation parameter value R_l. Results are summarized in Table I, and the comparison between theoretical and experimental data is shown in Fig. 4. Also, we consider a small frequency shift of 18 kHz in numerical simulations to match the resonance curves. This effect may originate from some small capacitive and/or inductive contributions that we have not previously taken into account.

Thus, with a consistent set of parameter values, and using again elementary circuit theory, we describe the full electric line of N coupled single cell elements by the following system of coupled ordinary differential equations:

$$\begin{aligned} c(v_n)\frac{dv_n}{d\tau} &= y_n - i_D(v_n) + \frac{\cos(\Omega\tau)}{RC_0\omega_0} - \left(\frac{1}{R_l}+\frac{1}{R}\right)\frac{v_n}{\omega_0 C_0}, \\ \frac{dy_n}{d\tau} &= \frac{L_2}{L_1}(v_{n+1}+v_{n-1}-2v_n) - v_n, \end{aligned} \tag{5}$$

where all magnitudes are in dimensionless units. Within this nonlinear dynamical lattice model, our waveforms of interest, namely the discrete breathers, are calculated as fixed points of the map

$$\begin{bmatrix} v_n(0) \\ \frac{dv_n}{d\tau}(0) \\ y_n(0) \\ \frac{dy_n}{d\tau}(0) \end{bmatrix} \rightarrow \begin{bmatrix} v_n(T) \\ \frac{dv_n}{d\tau}(T) \\ y_n(T) \\ \frac{dy_n}{d\tau}(T) \end{bmatrix}, \tag{6}$$

where $T = 1/f$ is the temporal period of the breather. In order to study the linear stability of discrete breathers, we introduce a small perturbation (ξ_n, η_n) to a given solution (v_{n0}, y_{n0}) of

TABLE I. Values of the resistance R_l corresponding to different voltage amplitudes for the driving source V_d.

V_d (V)	1	2	3	4	5
R_l (Ω)	15 000	10 000	6000	5000	4500

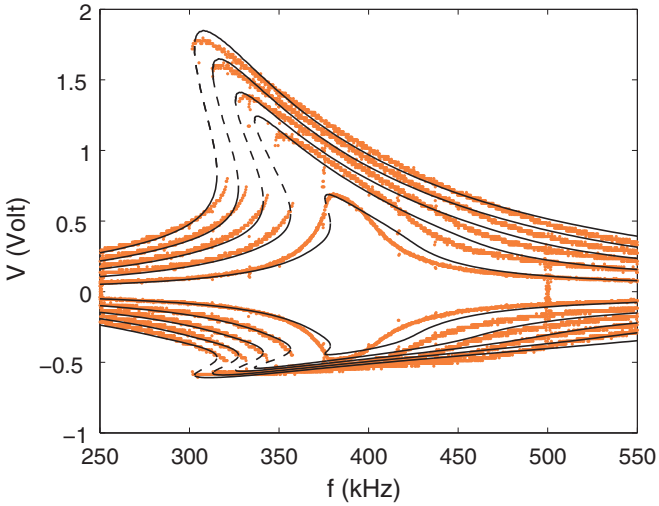

FIG. 4. (Color online) Nonlinear resonance curves corresponding to a single element. Dots (orange/gray) correspond to experimental data while the continuous and dashed black lines correspond, respectively, to stable and unstable numerical solutions. From bottom to top: $V_d = 1$, 2, 3, 4, and 5 V.

Eq. (6) according to $v_n = v_{n0} + \xi_n$, $y_n = y_{n0} + \eta_n$. Then, the equations satisfied to first order by (ξ_n, η_n) are

$$\begin{aligned} c(v_{n0})\frac{d\xi_n}{d\tau} &= \eta_n - \Gamma(v_{n0};t)\xi_n, \\ \frac{d\eta_n}{d\tau} &= \frac{L_2}{L_1}(\xi_{n+1}+\xi_{n-1}-2\xi_n) - \xi_n \end{aligned} \tag{7}$$

with $\Gamma(v_{n0};t)$ being

$$\begin{aligned} &\Gamma(v_{n0};t) \\ &= \frac{di_D(v_{n0})}{dv_{n0}} + \left(\frac{1}{R_l}+\frac{1}{R}\right)\frac{1}{\omega_0 C_0} + \frac{d\ln[c(v_{n0})]}{dv_{n0}} \\ &\quad\times\left[y_{n0} - i_D(v_n 0) + \frac{\cos(\Omega\tau)}{RC_0\omega_0} - \left(\frac{1}{R_l}+\frac{1}{R}\right)\frac{v_{n0}}{\omega_0 C_0}\right]. \end{aligned}$$

To identify the orbital stability of the relevant solutions, a Floquet analysis can be performed. Then, the stability properties are given by the spectrum of the Floquet operator $\mathcal{M}$ (whose matrix representation is the monodromy) defined as

$$\begin{bmatrix} \xi_n(T) \\ \frac{d\xi_n}{d\tau}(T) \\ \eta_n(T) \\ \frac{d\eta_n}{d\tau}(T) \end{bmatrix} = \mathcal{M}\begin{bmatrix} \xi_n(0) \\ \frac{d\xi_n}{d\tau}(0) \\ \eta_n(0) \\ \frac{d\eta_n}{d\tau}(0) \end{bmatrix}. \tag{8}$$

The $4N \times 4N$ monodromy eigenvalues λ are called the *Floquet multipliers*. If the breather is stable, all the eigenvalues lie inside the unit circle.

III. NUMERICAL COMPUTATIONS AND EXPERIMENTAL RESULTS

Using Eq. (6) we have generated n-peak ILMs and determined numerically their stability islands in (V_d, f) parameter space. We have found that there exist overlapping regions where two or several of these n-peak configurations exist and are stable. Therefore, the long-term dynamics in these regions

is chiefly dependent on initial conditions. However, determining precisely the basins of attraction of each configuration is not possible because of the high dimensionality of the problem.

Figure 5 shows the existence and stability diagrams for one-, two-, and three-peak breathers. The values of R_l are obtained through cubic interpolation from Table I. Notice that the lattice allows different configurations of solutions of n-peak breathers for $n > 1$ corresponding to the peaks centered at different locations, but determining precisely the diagrams corresponding to all possible configurations is not possible because of the size of the lattice. Therefore, we have studied only breathers with peaks as far apart as possible.

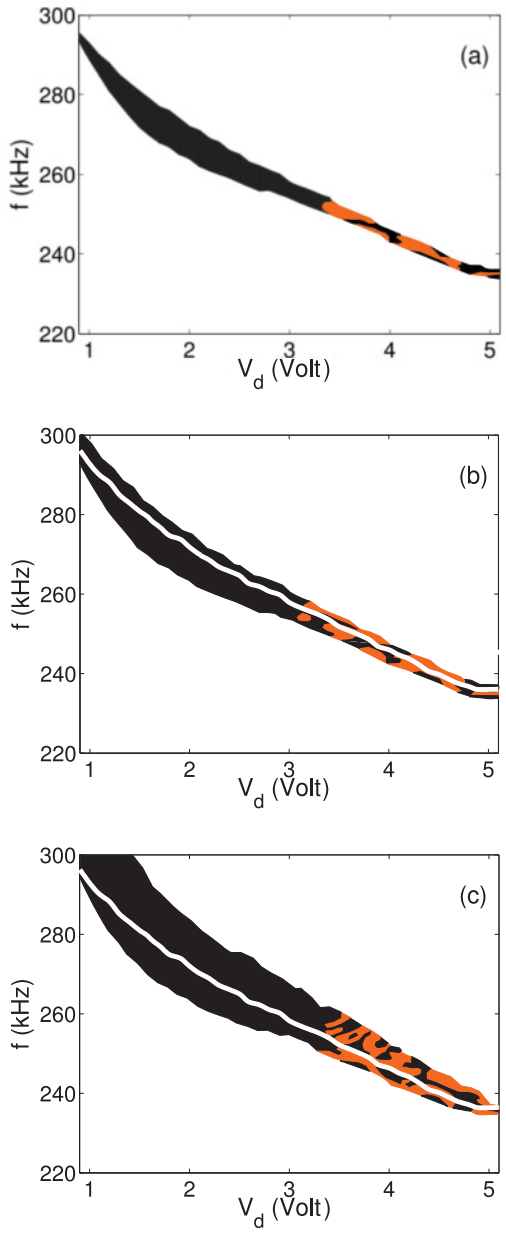

FIG. 5. (Color online) Existence islands for n-peak breathers. The white line denotes the threshold where the homogeneous state becomes unstable (above the line). Black areas correspond to stable solutions and orange (gray) areas to unstable solutions. (a) One-peak breather (the homogeneous state threshold is located at the top border of the areas), (b) a family of two-peak breather, and (c) a family of three-peak breathers. All data correspond to numerical simulations.

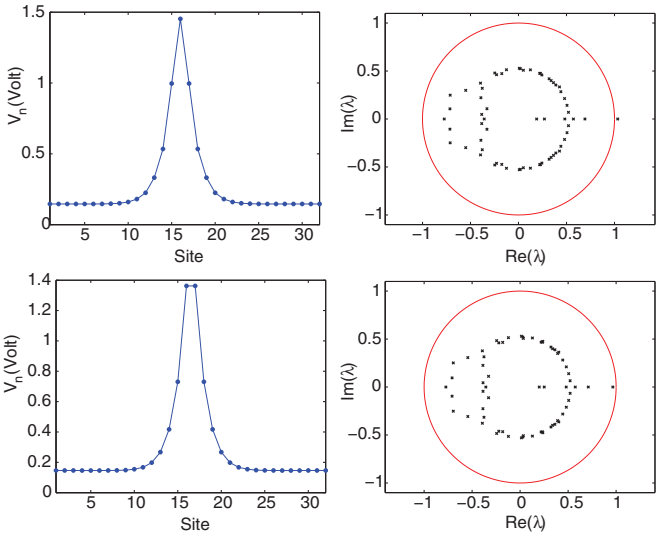

FIG. 6. (Color online) Breather profiles (left column) and corresponding Floquet multiplier spectra (right column) for $\tau = 0$, $V_d = 4$ V, and $f = 243.6$ kHz. The top (bottom) panels correspond to the unstable (stable) one-site (intersite) breather. All data correspond to numerical simulations.

Remarkably, breathers are generally robust for $V_d \lesssim 3$ V. Above that critical value, the considered solutions may become unstable in some "instability windows" (see orange/gray regions). Those instabilities, which are of exponential kind, typically lead an onsite breather profile to deform into a stable intersite breather waveform. We have analyzed in more detail the dependence of those instabilities for one-peak breathers. The study for higher peaked structure is cumbersome due to the increasing number of intersite structures that might arise. Figure 6 shows an example of one-peaked onsite and intersite breathers together with their Floquet spectrum.

A detailed analysis shows that for $3 \lesssim V_d \leqslant 5$ V, intersite breathers are always stable, whereas onsite ones may be unstable (i.e., there is no stability exchange as it occurs in Klein-Gordon lattices). However, for $V_d \lesssim 2$ V, intersite breathers are always unstable, whereas onsite breathers are stable. Finally, for $2\text{ V} \lesssim V_d \lesssim 3$ V, intersite breathers experience instability windows, whereas their onsite counterparts are stable. Figures 7–9 illustrate a typical set of relevant results for the cases of $V_d = 1.5$ V, $V_d = 2.5$ V, and $V_d = 4$ V which summarize the different possible regimes as V_d is varied. The unity crossings indicated by the red line (wherever relevant) in the right panel of each of the figures mark the stability changes of the pertinent solutions.

We have also performed an analysis of the stability of one-peak breathers for larger lattices ($N = 101$) and observe that the existence and stability range for onsite and intersite breathers are not significantly altered.

To corroborate the numerical picture, we have also performed an analogous experimental analysis. To determine experimentally the stability islands, we have chosen a particular voltage V_d and, starting at low frequencies (homogeneous state), and increasing f adiabatically, we can reach different

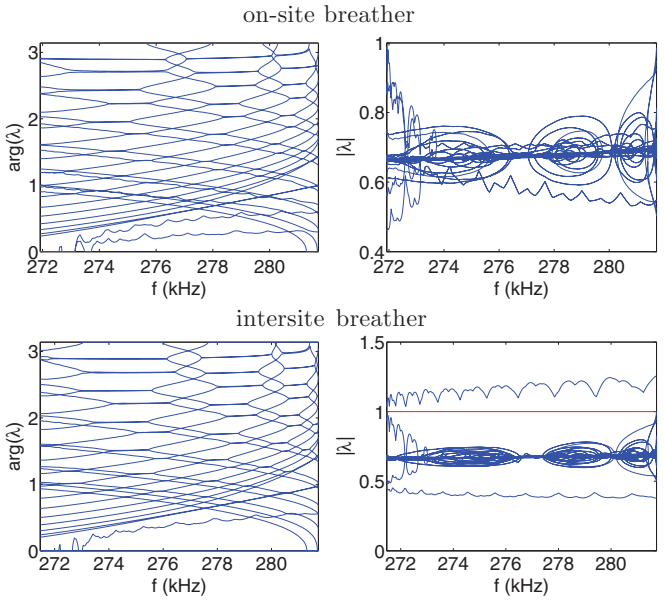

FIG. 7. (Color online) Dependence of the Floquet multipliers on the frequency for $N = 32$ cells and $V_d = 1.5$ V. The top (bottom) row of panels corresponds to the onsite (intersite) breather. The left and right column of panels depicts, respectively, the argument and magnitude of the Floquet multipliers. The horizontal (red) line in the spectra depicts the stability threshold. All data correspond to numerical simulations.

regions. Going up and down adiabatically we are able to examine regions of coexistence between different n-peak breathers. In particular, regions corresponding to one-peak, two-peak, and three-peak breathers have been detected experimentally. The three-peak region is bounded from above by the four- and five-peak areas, which we did not track. We have determined the boundaries by doing up-sweeps and down-sweeps, with significant hysteresis phenomena.

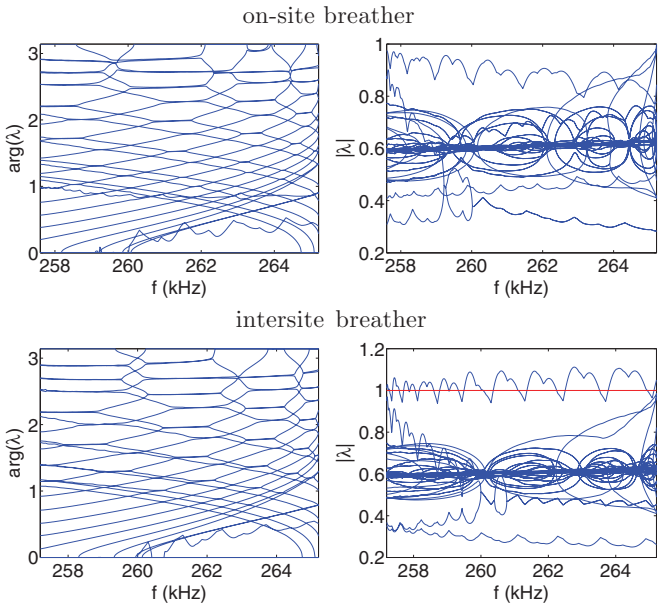

FIG. 8. (Color online) Same as Fig. 7 but for $V_d = 2.5$ V.

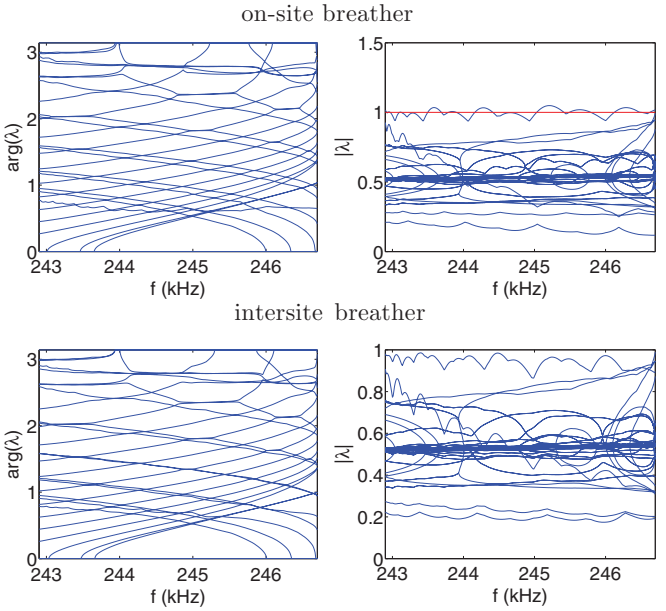

FIG. 9. (Color online) Same as Fig. 7 but for $V_d = 4$ V.

It should be mentioned that for the interior of the one-peak region, we demonstrated experimentally that the discrete breather and ILM can be centered at any node in the lattice and survive there. This verification implies that the experimental lattice—despite its inherent component variability—does display a sufficient degree of spatial homogeneity for the basic localization phenomenon to be considered (discrete) translationally invariant. In practice, we employed an impurity in the form of an external inductor physically touching a L_2 lattice inductor to make the ILM hop to that impurity site because of the existence of an impurity mode localized around the impurity site (see Fig. 10). Upon removing the impurity, the ILM would then persist at that site. We believe

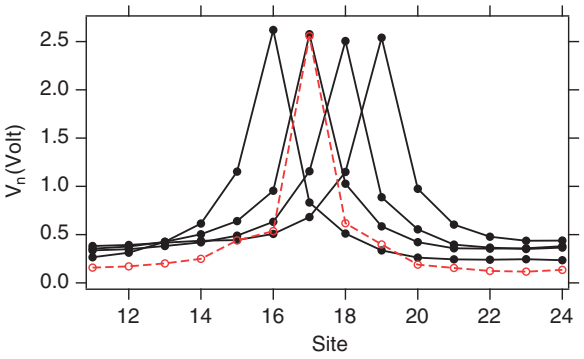

FIG. 10. (Color online) The ILM can exist at any site of the lattice; here $f = 253$ kHz and $V_d = 4$ V. We demonstrate that the ILM can be made to jump to the neighboring site upon the temporary creation of an impurity there. The left-most profile (centered at site 16) turns into the dotted (red) trace when an external inductor is placed in the direct vicinity of the L_2 inductor at site 17. Upon removal of this external inductor, the ILM persists at site 17 (solid black trace). This process can be repeated to move the ILM further to the right, as shown. All data correspond to experiments.

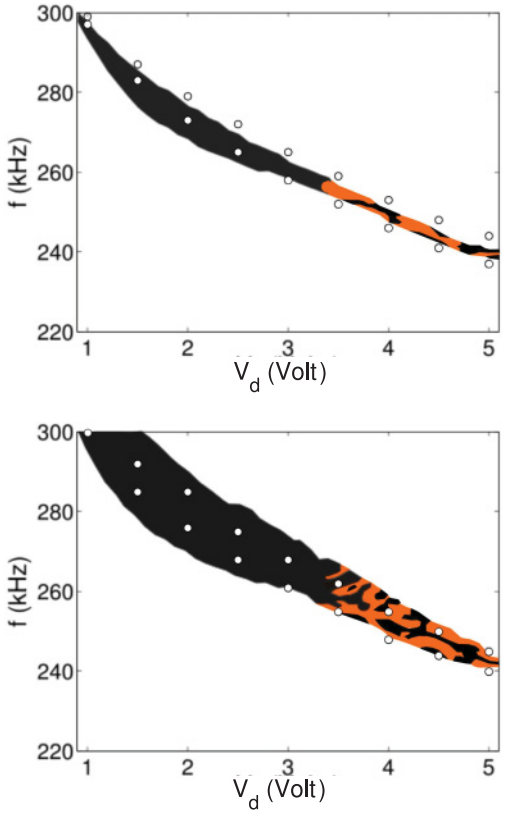

FIG. 11. (Color online) Existence regions of one-peaked (top panel) and a family of three-peaked (bottom panel) breathers obtained numerically (black areas correspond to stable solutions and orange/gray one to unstable solutions) as compared to experimental data identifying the range of observations of the corresponding type of states (circles). The theoretical data are displaced by a +7 kHz frequency offset.

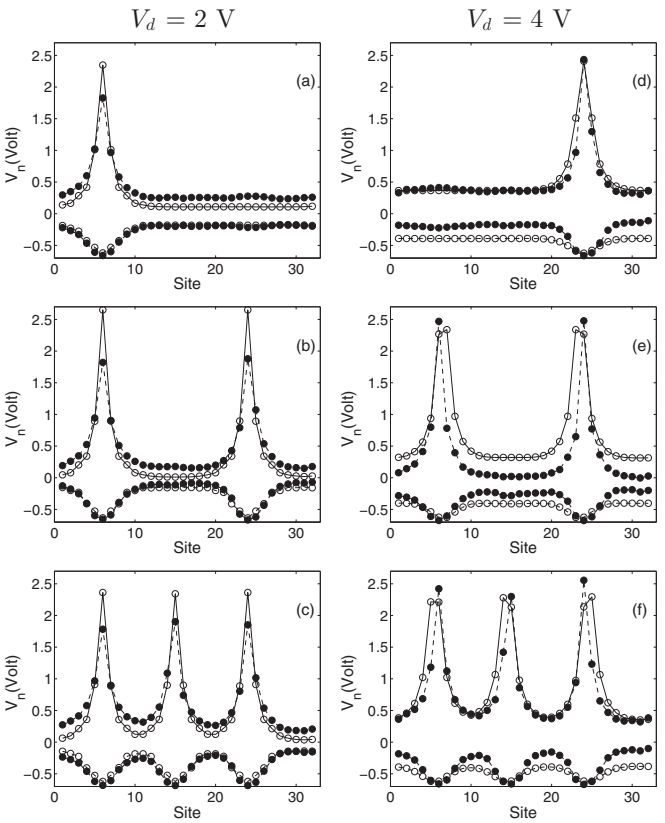

FIG. 12. Experimental (•) and numerical (○) one-, two-, and three-peak breather profiles for different driver voltage V_d and frequencies values. The left (right) column of panels corresponds to a driver strength $V_d = 2$ V ($V_d = 4$ V). Each panel correspond to the following experimental (f_{expt}) and numerical (f_{num}) driving frequencies in kHz: (a) $(f_{\text{expt}}, f_{\text{num}}) = (275,268)$, (b) $(f_{\text{expt}}, f_{\text{num}}) = (276,269)$, (c) $(f_{\text{expt}}, f_{\text{num}}) = (280,273)$, (d) $(f_{\text{expt}}, f_{\text{num}}) = (248,244)$, (e) $(f_{\text{expt}}, f_{\text{num}}) = (254,247)$, and (f) $(f_{\text{expt}}, f_{\text{num}}) = (249,245)$.

that this technique could prove extremely valuable toward the guidance and manipulation (essentially, at will) of the ILMs in this system. The ability to controllably move localized energy around the lattice could, for instance, facilitate future experiments on breather-breather interactions. Moreover, not only can ILMs be shepherded in this manner, but we can also use the same technique to "seed" an ILM at a location of our choice; this is possible for driving frequencies just below those for which the modulational instability spontaneously produces localization patterns. In this way we can generate breathers at any time and any location in the lattice, depending only on where and when the impurity is briefly introduced.

A comparison between theoretical and experimental data of one-peak and three-peak breathers is shown in Fig. 11. The precise width of any stability region is hard to match because there exist regions of different peak numbers and regions of different families with the same number of peaks overlap, and thus their competition prevents an absolutely definitive picture. Which one "wins" out appears to depend sensitively on small lattice impurities present in our (commercial) experimental elements. For instance, in the experiment it looks as if the two-peak region is squeezed in favor of the one-peak region. This might be the reason why the experimental one-peak region is slightly wider at higher driver amplitudes than it appears in the corresponding theoretical predictions. Nonetheless, the comparison between experimental and theoretical existence regions depicted in Fig. 11 shows generally good qualitative (and even quantitative) agreement in the context of the proposed model.

More detailed experimental results are shown in Fig. 12 where we depict peak profiles at two different driver voltages. The profiles were taken at the times of largest peak voltage amplitude and lowest peak voltage amplitude. For $V_d = 2$ V (left column of panels) we see that, as the frequency is raised from below, we cross from the one-peak region through the two-peak region and into the three-peak region. For the $V_d =$ 4 V case (right column of panels) the same sequence can be observed when scanning in one frequency direction. In order to illustrate both the hysteresis and the overlap between n-peak regions, we depict in Figs. 12(e) and 12(f) a situation where the two-peak solution occurs at a higher frequency than the three-peaked one. The reason is that in Fig. 12(f) the three-peak solution was obtained at higher frequencies and then

adiabatically extended to lower ones, whereas in Fig. 12(e) the two-peak solution was obtained starting from the one-peak region.

We show the eventual location of peaks in the breather pattern (i.e., after the driver has been on for a long time). However, it is important to mention that the exact location where the peaks eventually settle is sensitive to slight impurities in the lattice. We have noticed that when we turn on the voltage source, at first we can observe a more sinusoidal pattern (corresponding to the most modulationally unstable k value), but as the pattern reaches higher energy and becomes more nonlinear, the peaks may shift and adjust themselves in the lattice. As it can be observed, the peaks are not perfectly equispaced in the lattice. This is due to the inhomogeneities present in the experiment.

For the numerical results depicted in Fig. 12 we used a set of initials conditions based on the experimental data and determined the stationary state by letting the numerical profiles settle to a steady state. For the cases corresponding to $V_d = 2$ V and $V_d = 4$ V, adding a small frequency offset $\Delta f \approx 4$–7 kHz, we observe, in general, a good agreement between numerics and experimental data. The mismatch between experiments and theory, in particular the intersite distance peaks, can be attributed to the above mentioned factors. Furthermore, to reproduce precisely the experimental peak voltage is extremely difficult because it corresponds to the voltage at resonance and, therefore, even very small parameter changes can create large differences in the maximum amplitudes. Nevertheless, the quantitative agreement appears fairly good, especially for the $V_d = 4$ V case.

IV. CONCLUSIONS

In this paper we have formulated a prototypical model that is able to describe the formation of nonlinear intrinsic localized modes (or discrete breathers) in an experimental electric line. This has been derived based on a combination of the fairly accurate characterization of a single element within the lattice (including its nonlinear resonance curves and hysteretic behavior) and fundamental circuit theory in order to properly couple the elements. Comparison between theory and experiments shows very good qualitative and even good quantitative agreement between the two. We characterized the regions of existence and stability of n-peaked breathers for $n = 1, 2, 3$ and illustrated how transitions of the coherent waveforms of one kind to those of another kind take place, rationalizing them on the basis of stability properties and their corresponding Floquet spectra. We also showed that the precise number of peaks and their location in the lattice is fairly sensitive to initial conditions, a feature also generally observed in the experiments where the potential for states with different numbers of peaks similarly manifests.

The level of interplay between theory and experiment achieved in this study is beneficial from a number of larger scale perspectives. First, it allows us to better investigate and identify which aspects of the single-cell characteristics are essential for the emergence of the collective phenomenon of localization in the lattice. We see, for instance, that an exact match of the diode properties is not necessary to capture the essence of self-localization in the lattice and, furthermore, to match the experimental ILM profiles very well. On the other hand, some diode characteristics were found to be essential for the manifestation of these nonlinear phenomena, such as the large curvature in the $C(V)$ curve around the origin. Experimentally, too, we observe the disappearance of ILMs when the diodes are reverse biased too much and the $C(V)$ curvature diminishes. Second, the success in recovering numerically the main experimental observations demonstrates that these lattice effects are really derivable from and contained within the basic circuit equations and do not rely on some hidden feature of the experimental system. This cements the value of the theoretical modeling as a useful tool to potentially explore interesting and relevant phenomenologies within this system, including its response to different types of external drive and its generalizations to higher dimensional setups. Finally, while the experimental observation first motivated the numerical study, it then helped shape the model and tie down relevant parameter values, the numerical and theoretical study also uncovered aspects missed by the experiments, such as the stability of intersite breathers at larger driver amplitudes; more broadly, it places the empirical evidence into a broader dynamical-systems context. Conversely, the experimental investigation can sometimes yield unexpected results that would have been difficult to predict *a priori*, such as the possibility of moving breathers upon a slight modification of the unit cell [17]. The above constructive interplay and possibility for continuous feedback between theory and modeling and experiment is, arguably, one of the major advantages of the present nonlinear lattice system and one of the fundamental contributions of the present study.

Naturally, many directions of potential future research stem from the fundamental modeling and computation basis explored in the present manuscript. On the one hand, it would be very interesting to attempt to understand the stability properties of the different breather states from a more mathematical perspective, although this may admittedly prove a fairly difficult task. On the other hand, from the modeling and computation perspective in conjunction with experimental progress, the present work paves the way for potentially augmenting these systems into higher dimensional setups and attempting to realize discrete soliton as well as more complex discrete vortex states therein [2,18]. Such studies will be deferred to future publications.

ACKNOWLEDGMENTS

F.P. and J.C. acknowledges sponsorship by the Spanish MICINN under Grant No. FIS2008-04848. R.C.G. gratefully acknowledges the hospitality of the Grupo de Física No Lineal (GFNL, University of Sevilla, Spain) and support from NSF-DMS-0806762, Plan Propio de la Universidad de Sevilla, Grant No. IAC09-I-4669 of Junta de Andalucia and Ministerio de Ciencia e Innovación, Spain. P.G.K. acknowledges the support from NSF-DMS-0806762, NSF-CMMI-1000337, and from the Alexander von Humboldt, as well as the Alexander S. Onassis Public Benefit Foundation.

[1] S. Aubry, Physica D **103**, 201 (1997); R. S. MacKay, Physica A **288**, 174 (2000); D. K. Campbell, S. Flach, and Yu. S. Kivshar, Phys. Today **57**(1), 43 (2004).
[2] S. Flach and C. R. Willis, Phys. Rep. **295**, 181 (1998); S. Flach and A. V. Gorbach, *ibid*. **467**, 1 (2008).
[3] A. J. Sievers and S. Takeno, Phys. Rev. Lett. **61**, 970 (1988); J. B. Page, Phys. Rev. B **41**, 7835 (1990).
[4] R. S. MacKay and S. Aubry, Nonlinearity **7**, 1623 (1994).
[5] U. T. Schwarz, L. Q. English, and A. J. Sievers, Phys. Rev. Lett. **83**, 223 (1999).
[6] B. I. Swanson, J. A. Brozik, S. P. Love, G. F. Strouse, A. P. Shreve, A. R. Bishop, W. Z. Wang, and M. I. Salkola, Phys. Rev. Lett. **82**, 3288 (1999).
[7] Y. S. Kivshar and G. P. Agrawal, *Optical Solitons: From Fibers to Photonic Crystals* (Academic, San Diego, CA, 2003).
[8] E. Trias, J. J. Mazo, and T. P. Orlando, Phys. Rev. Lett. **84**, 741 (2000); P. Binder, D. Abraimov, A. V. Ustinov, S. Flach, and Y. Zolotaryuk, *ibid*. **84**, 745 (2000).
[9] M. Sato, B. E. Hubbard, and A. J. Sievers, Rev. Mod. Phys. **78**, 137 (2006).
[10] G. Theocharis, N. Boechler, P. G. Kevrekidis, S. Job, M. A. Porter, and C. Daraio, Phys. Rev. E **82**, 056604 (2010); N. Boechler, G. Theocharis, S. Job, P. G. Kevrekidis, M. A. Porter, and C. Daraio, Phys. Rev. Lett. **104**, 244302 (2010).
[11] M. Peyrard, Nonlinearity **17**, R1 (2004).
[12] J. P. Wrubel, M. Sato, and A. J. Sievers, Phys. Rev. Lett. **95**, 264101 (2005); M. Sato, B. E. Hubbard, and A. J. Sievers, Rev. Mod. Phys. **78**, 137 (2006); M. Kimura and T. Hikihara, Chaos **19**, 013138 (2009); J. Wiersig, S. Flach, and K. H. Ahn, Appl. Phys. Lett. **93**, 222110 (2008); M. Sato, S. Yasui, M. Kimura, T. Hikihara, and A. J. Sievers, Europhys. Lett. **80**, 30002 (2007).
[13] P. Marquie, J. M. Bilbault, and M. Remoissenet, Phys. Rev. E **49**, 828 (1994).
[14] M. Remoissenet, *Waves Called Solitons: Concepts and Experiments* (Springer, Berlin, 1999).
[15] R. Stearret and L. Q. English, J. Phys. D **40**, 5394 (2007).
[16] L. Q. English, R. B. Thakur, and R. Stearrett, Phys. Rev. E **77**, 066601 (2008).
[17] L. Q. English, F. Palmero, A. J. Sievers, P. G. Kevrekidis, and D. H. Barnak, Phys. Rev. E **81**, 046605 (2010).
[18] P. G. Kevrekidis, *The Discrete Nonlinear Schrödinger Equation: Mathematical Analysis, Numerical Computations and Physical Perspectives* (Springer, Heidelberg, 2009).